# REPORT DOCUMENTATION PAGE

*Form Approved*
*OMB No. 0704-0188*



| 1. REPORT DATE (DD-MM-YYYY) | 2. REPORT DATE | 3. DATES COVERED: *(From – To)* |
|---|---|---|
| 20-12-2007 | 20-12-2007 | 24-03-06 - 30-09-07 |

**4. TITLE AND SUBTITLE**

Shock Processing of Bulk Anisotropic Nanocomposite Permanent Magnets

**5a. CONTRACT NUMBER**
N00014-06-1-0545

**5b. GRANT NUMBER**

**5c. PROGRAM ELEMENT NUMBER**

**6. AUTHOR(S)**

Naresh Thadhani and Christopher Wehrenberg

**5d. PROJECT NUMBER**

**5e. TASK NUMBER**

**5f. WORK UNIT NUMBER**

**7. PERFORMING ORGANIZATION NAME(S) AND ADDRESS(ES)**
Georgia Institute of Technology
771Ferst Drive, Atlanat, GA 30332-0245

**8. PERFORMING ORGANIZATION REPORT NUMBER**

**9. SPONSORING/MONITORING AGENCY NAME(S) AND ADDRESS(ES)**
JULIE CHRISTODOULOU
ONR
875 NORTH RANDOLPH STREET
ARLINGTON
VA 22203-1995
USA

**10. SPONSOR/MONITOR'S ACRONYM(S)**

**AGENCY REPORT NUMBER**

**12. DISTRIBUTION AVAILABILITY STATEMENT**
public availability

**13. SUPPLEMENTARY NOTES**

**14. ABSTRACT**
Shock-processing of precursor powders has been employed for fabricating bulk anisotropic nanocomposite permanent magnets. While our prior work de shock compaction can be employed to fabricate bulk exchange-coupled nanocomposite (RE2Fe14B/α-Fe) magnets in the form of discs and rods, the e (BH)max was limited to 17.8 MGOe due to the isotropic structure of the magnet. In this work we have used high-strain-rate deformation concomitant wit compaction employing the single-stage gas gun to make bulk nanocomposite powder compacts, while retaining the nano-scale structure of the hard an phases, and generating magnetic anisotropy due to texture introduced via severe plastic deformation. Two methods have been investigated. In one cas powder compact held against a rigid anvil plate is deformed upon impact by a projectile such that it is forged in the shape of a disc. In another case, the powder compact is dynamically extruded through an angular die to achieve reductions in cross-section of greater than 100%. Two- and three-dimension simulations are employed to design shock compression geometries and to predict impact conditions that result in complete powder densification and va texture introduced during dynamic forging and extrusion. The microstructure of the recovered compacts, including hard/soft phase grain size and hard p characterized, and correlated with magnetic property measurements. The seed project is an attempt to demonstrate the ability to employ high-strain-rat deformation for introducing magnetic anisotropy in otherwise difficult-to-deform magnetic materials, thereby making it possible to fabricate magnets with

**15. SUBJECT TERMS**
dynamic densification, forging, and extrusion; permanent magnets; exchange-coupling

| 16. SECURITY CLASSIFICATION OF: | | | 17. LIMITATION OF ABSTRACT | 18. NUMBER OF PAGES | 19a. NAME OF RESPONSIBLE PERSON |
|---|---|---|---|---|---|
| a. REPORT | b. ABSTRACT | C. THIS PAGE | | | Naresh Thadhani |
| U | U | U | U | 14 | 20b. TELEPHONE NUMBER (include area code) 404-894-2651 |

INSTRUCTONS FOR COMPLETING SF 298

**1. REPORT DATE**. Full publication date, including day, month, if available. Must cite at least the year and be Year 2000 compliant, e.g., 30-06-1998; xx-08-1998, xx-xx-1998.

**2. REPORT TYPE**. State the type of report, such as final, technical, interim, memorandum, master's thesis, progress, quarterly, research, special, group study, etc.

**3. DATES COVERED**. Indicate the time during which the work was performed and the report was written, e.g., Jun 1998; 1-10 Jun 1996; May – Nov 1998; Nov 1998.

**4. TITLE.** Enter title and subtitle with volume number and part number, if applicable. On classified documents, enter the title classification in parentheses.

**5a. CONTRACT NUMBER.** Enter all contract numbers as they appear in the report, e.g. F33615-86-C-5169

**5b. GRANT NUMBER.** Enter all grant numbers as they appear in the report, e.g. 1F665702D1257.

**5c. PROGRAM ELEMENT NUMBER.** Enter all program element numbers as they appear in the report, e.g. AFOSR-82-1234

**5d. PROJECT NUMBER**. Enter project numbers as they appear in the report, e.g. 1F665702D1257

**5e. TASK NUMBER**. Enter all ask numbers as they appear in the report, e.g. 05; RF0330201; T4112.

**5f. WORK UNIT NUMBER.** Enter all work unit numbers as they appear in the report, e.g. 001; AFAPL30480105

**6. AUTHOR(S).** Enter name(s) of person(s) responsible for writing the report, performing the research, or credited with the content of the report. The form of entry is the latest name, first name, middle initial, and additional qualifiers separated by commas, e.g. Smith, Richard, Jr.

**7. PERFORMING ORGANIZATION NAME(S) AND ADDRESS(ES).** Self – explanatory.

**8. PERFORMING ORGANIZATION REPORT NUMBER.** Enter all unique alphanumeric report numbers assigned by the performing organization, e.g. BRL-1234; AFWL-TR-85-4017-Vol-21-PT-2.

**9. SPONSORING/MONITORS AGENCY NAME(S) AND ADDRESS(ES**). Enter the name and address of the organization(s) financially responsible for and monitoring the work.

**10. SPONSOR/MONITOR'S ACRONYM(S).** Enter, if available, e.g. BRL, ARDEC, NADC

**11. SPONSOR/MONITOR'S REPORT NUMBER(S).** Enter report number as assigned by the sponsoring/monitoring agency, if available, e.g. BRL-TR-829; - 215

**12. DISTRIBUTION/AVAILABILITY STATEMENT.** Use agency-mandated availability statements to indicate the public availability or distribution limitations of the report. If additional limitations/restrictions or special markings are indicated, follow agency authorization procedures, e.g. RD/FRD, PROPIN, ITAR, etc. Include copyright information.

**13. SUPPLEMENTARY NOTES.** Enter information not included elsewhere such as: prepared in cooperation with; translation of; report supersedes; old edition number, etc.

**14. ABSTRACT.** A brief (approximately 200 words) factual summary of the most significant information.

**15. SUBJECT TERMS.** Key words or phrases identifying major concepts in the report.

**16. SECURITY CLASSIFICATION**. Enter security classification in accordance with security classification regulations, e.g. U, C, S, etc. If this form contains classified information, stamp classification level on the top and bottom of this page.

**17. LIMITATION OF ABSTRACT**.

This block must be completed to assign a distribution limitation to the abstract. Enter UU (Unclassified Unlimited) or SAR (Same as Report). An entry in this block is necessary if the abstract is to be limited.

**Final Technical Report**

# Shock Processing of Bulk Anisotropic Nanocomposite Permanent Magnets

Submitted to

Dr. Julie Christodoulou
Office of Naval Research
875 North Randolph Street
Arlington, VA 22203-1995

Prepared by:

Naresh N. Thadhani (P.I.) and Christopher Wehrenberg (Ph.D. student)
School of Materials Science and Engineering,
Georgia Institute of Technology
771 Ferst Drive, Atlanta, GA 30332-0245
Tel: (404) 894-2651; Fax: (404) 894-1940;
Email: naresh.thadhani@mse.gatech.edu

December 20, 2007

**Final Technical Report**
**Shock Processing of Bulk Anisotropic Nanocomposite Permanent Magnets**

Naresh N. Thadhani (P.I.) and Christopher Wehrenberg (Ph.D. student)
School of Materials Science and Engineering, Georgia Institute of Technology
771 Ferst Drive, Atlanta, GA 30332-0245
Tel: (404) 894-2651; Fax: (404) 894-1940; Email: naresh.thadhani@mse.gatech.edu

## 1. Summary

Shock-processing of precursor powders has been employed for fabricating **bulk anisotropic nanocomposite permanent magnets.** While our prior work demonstrated that shock compaction can be employed to fabricate bulk exchange-coupled nanocomposite ($RE_2Fe_{14}B/\alpha$-Fe) magnets in the form of discs and rods, the energy product $(BH)_{max}$ was limited to 17.8 MGOe due to the **isotropic** structure of the magnet. In this work we have used high-strain-rate deformation concomitant with shock compaction employing the single-stage gas gun to make bulk nanocomposite powder compacts, while retaining the nano-scale structure of the hard and soft magnetic phases, and generating magnetic anisotropy due to texture introduced via severe plastic deformation.

Two methods have been investigated. In one case, a rod-shaped powder compact held against a rigid anvil plate is deformed upon impact by a projectile such that it is forged in the shape of a disc. In another case, the rod-shaped powder compact is dynamically extruded through an angular die to achieve reductions in cross-section of greater than 100%. Two- and three-dimensional numerical simulations are employed to design shock compression geometries and to predict impact conditions that result in complete powder densification and varying degrees of texture introduced during dynamic forging and extrusion. The microstructure of the recovered compacts, including hard/soft phase grain size and hard phase texture is characterized, and correlated with magnetic property measurements.

The seed project is an attempt to demonstrate the ability to employ high-strain-rate severe plastic deformation for introducing **magnetic anisotropy** in otherwise difficult-to-deform magnetic materials, thereby making it possible to fabricate magnets with high energy products.

## 2. Background, Motivation, and Problem Statement

### 2.1 Exchange coupled Nanocomposite Magnets

Nanocomposite magnets[i] based on exchange-coupled nanoscale hard and soft magnetic phases have attracted considerable attention due to the combination of high magnetocrystalline anisotropy possible in magnetically hard phase, $R_2Fe_{14}B$ (R=rare earth), and large saturation polarization of magnetically soft phase, α-Fe. Our past work in collaboration with Prof. Ping Liu, has utilized the advantages of microstructure control provided by shock consolidation, to fabricate bulk exchange-coupled nanocomposite magnets starting with melt-spun nanocomposite powders of $Pr_2Fe_{14}B$-based with 20wt%α-Fe. Dense compacts with ~99% of theoretical maximum density and nano-scale bimodal grain size distribution (with 20-25 nm and 10-15 nm grains) were produced with solid-state metallurgical bonding and no evidence of any detrimental phases at inter-particle and inter-phase regions. Complete densification and retention of nano structure ensured strong exchange coupling between hard/soft phases as revealed by a smooth hysteresis loop (shown in Fig. 1(a)) and high remanence ratio ($M_r/M_s$ ~ 0.63). The coercivity, $H_c$ was 6.45 kOe and energy product $(BH)_{max}$ was 13.9 MGOe (or 17.8 MGOe after correcting for demagnetization). Annealing the shock-consolidated compacts allowed further increase in coercivity (Fig. 1(b)) without affecting the energy product, indicating that post-compaction thermal treatments can be used to further optimize the magnetic properties. This is the first such demonstration of bulk exchange-coupled nanocomposite magnets fabricated as discs (10 mm diameter by 3 mm thickness) and rods (25 mm diameter by 150 mm length)[ii,iii].

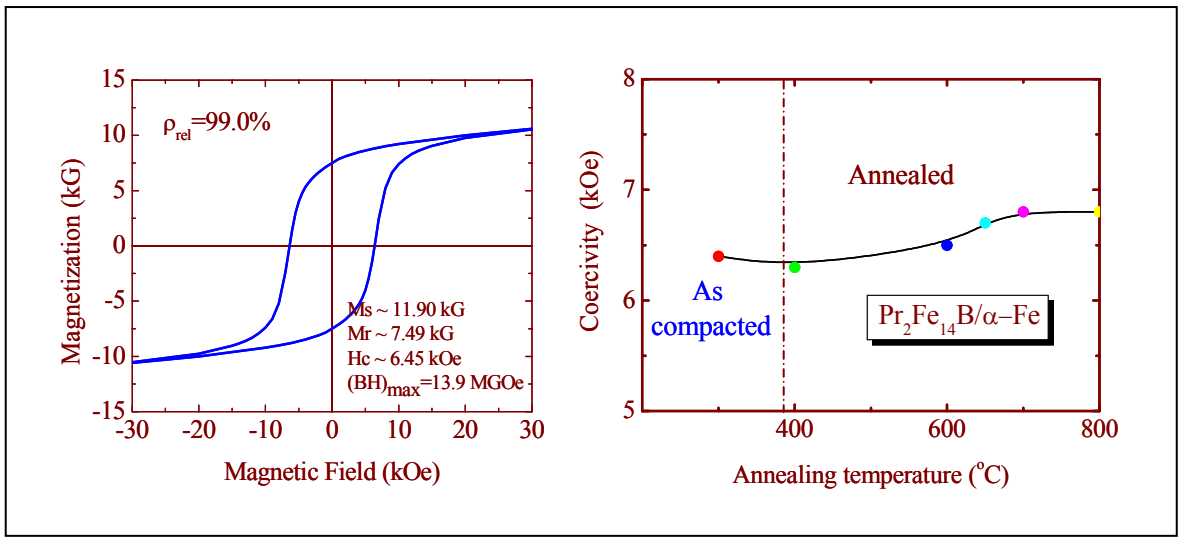


***Fig. 1**. (a) Shock consolidated $Pr_2Fe_{14}B$/α-Fe reveals smooth hysteresis loop indicating hard/soft phase exchange coupling. (b) Annealing shows magnetic property improvement with a peak in energy product at ~650°C.*

## 2.2 Problem Statement

While the energy product for the shock consolidated (and annealed) compacts fabricated in our prior work is higher than that for commercial resin bonded exchange-coupled permanent magnets (typical $(BH)_{max}$ ~8-12 MGOe), it is still significantly lower than what can be expected of nanocomposite permanent magnets. The low value was limited by the isotropic structure of the shock consolidated compacts. Epitaxial growth has often been used to obtain magnetocrystalline anisotropy in thin films, but fabrication of bulk compacts via pressing or sintering of powders, while attaining magnetic field alignment has been difficult. Another alternative to field alignment is to introduce structural texture via severe plastic deformation. However, the inherent brittleness of the ceramic (hard) magnetic phase makes it difficult to achieve the large deformations needed to generate texture. We therefore, have employed high-strain-rate (dynamic) severe plastic deformation processes to simultaneously compact and deform precursor powders, by exploiting the effects of dynamic plasticity, to make bulk highly textured hard/soft phase nanocomposite magnets.

The **goal** of this seed project was therefore, to demonstrate generation of magnetocrystalline anisotropy in $Pr_2Fe_{14}B$-20wt%$\alpha$-Fe nanocomposite compacts with texture introduced through severe plastic deformation and concomitant shock compaction via dynamic high-strain-rate forging and extrusion processes.

# 3. Technical Approach and Plan of Work

The approach for fabricating bulk anisotropic nanocomposite magnets is based on our experience with the use of the 80-mm diameter single stage gas gun for shock compaction of difficult-to-consolidate powders and for performing high-strain-rate deformation experiments for determining and validating the constitutive properties of armor/anti-armor materials. Two methods have been explored to simultaneously consolidate and severely plastically deform $Pr_2Fe_{14}B$-20wt%$\alpha$Fe nanocomposite powders using the gas gun:

(a) *Forging a rod-shaped compact into a disc, by impacting a rigid anvil plate (mounted on Al-sabot) on to a stationary rod-shaped compact held against a rigid target, and*

(b) *Dynamic extrusion of a rod-shaped powder compact through an angular die resulting in a greater than 100% reduction in cross-sectional area.*

With both methods, the experiments are conducted at impact velocities in the range of 500-1000 m/s. The desired impact conditions, including impact velocity and initial packing density are calculated based on previously established models of densification of the nanocomposite powders. Two-dimensional and three-dimensional numerical simulations using AUTODYN and CTH programs is used to design the experimental set-up, and the impactor and sample containment geometry, as well as to predict the impact conditions. The current experiment tank of the 80-mm gas gun was modified to permit building of geometries that allow sample containment in the case of the forging experiments. Safe recovery of the compacted and deformed materials following impact was ensured, with some modification of our experiment

tank.A new 0.3 cal gas gun was also acquired to permit extrusion experiments. The compacted (and forged or extruded) materials were characterized with respect to their detailed microstructure and magnetic properties. Microstructural characterization was performed using the facilities available at Georgia Tech, to determine the degree of densification, retention of the nano-scale structure, and formation of crystalline texture. Magnetic property characterization were performed in collaboration with Prof. Ping Liu at University of Texas in Arlington.

## 3.1 Materials Systems investigated

Early work focused on $Pr_2Fe_{14}B$-20wt%α-Fe nanocomposite flake-shaped powders obtained from ground melt-spun ribbons, available through Magnaquench, Inc. The particles of ~20 μm thickness, as shown in the SEM image in Fig. 2(a), are polycrystalline nanocomposites, of 15-25 nm hard/soft phase grains, as illustrated by the dark-field TEM image in Fig. 2(b). The flake-shaped particles enable attaining high initial packing density (~70% TMD), which helps in limiting the thermal build-up during shock compression, thereby making it possible to achieve full densification without loss of the starting nano-scale grain size of the hard/soft magnetic phases. $SmCo_5$ powder was also obtained from Alfa Aesar Co. The particle size distribution is between 1-50 μm, while the grain size is from 1-5 μm, as seen in the Fig 3.

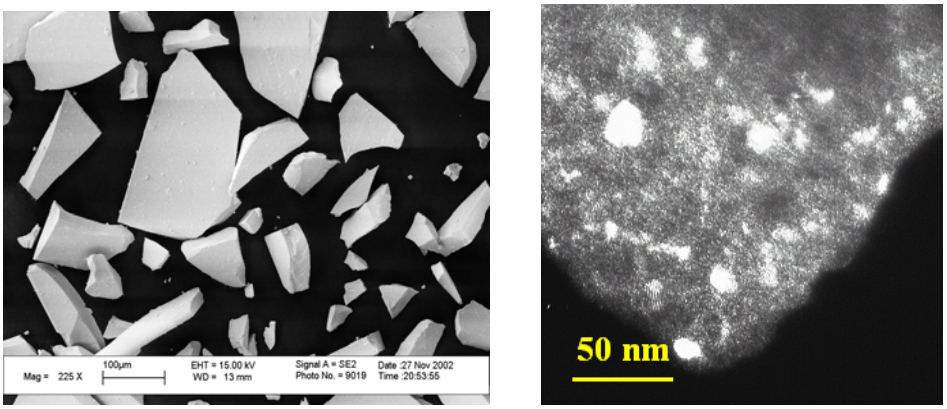


*Fig.2. (a) SEM image showing flake-shaped morphology of polycrystalline $Pr_2Fe_{14}B$-20wt%αFe powders obtained from melt-spun ribbons produced by Magnaquenc, (b) TEM dark-field image showing nano-sized (15-25 nm average size) hard/soft phases.*

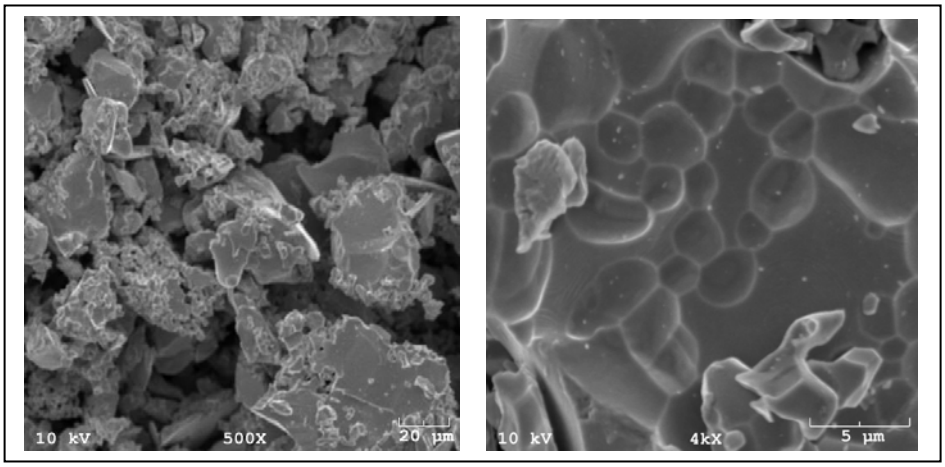


Fig. 3. SEM micrographs of staring powder morphology at 500X (Left) and sub-grain structure at 4000X (Right)

### 3.2 Dynamic Forging Experiments

Dynamic forging experiments concomitant with shock compaction was performed using our 80 mm diameter single stage gas gun with a projectile and target geometry illustrated in Figure 4. A rod-shaped powder compact (pressed in a copper or aluminum tube) was held against a rigid target plate, backed by an anvil anchor plate. Dynamic forging was achieved by impacting the powder compact with a projectile consisting of a rigid anvil plate mounted on an Al-sabot, and accelerated with compressed He gas at 500-1000 m/s.

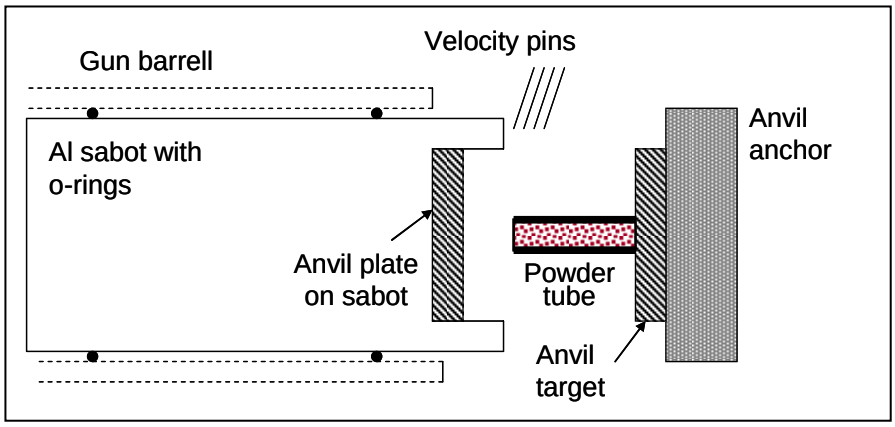


*Fig. 4. Sabot/target geometry for dynamic forging experiments.*

The sabot-target geometry was designed such that the radial deformation and plastic flow of the stationary rod-shaped powder compact held against the rigid anvil target occurs in a way that it becomes encapsulated between the anvil plates and the surrounding sabot. The impact velocity is monitored using time-of-arrival velocity pins which are mounted on the muzzle where the projectile exits the gas gun barrel. The desired impact velocity is determined as a function of the initial packing powder density and calculations based on previously established models of densification of the nanocomposite powders. In other words, the lower bound of impact velocity is derived based on pressure needed to reach full densification $\{P_y \sim 3\sigma_y \rho^2 (\rho-\rho_o)/(1-\rho_o)\}$, and the upper bound is based on the pressure needed to reduce the rod to disc form with a reversed aspect ratio $\{P_y \sim \sigma_y \exp(2\mu a/h)\}$. In these equations, $\sigma_y$ is the average yield strength, $\rho_o$ and $\rho$ are initial and final fractional densities, $\mu$ is coefficient of friction, $a$ is diameter and $h$ is sample height/thickness. Two- and three-dimensional numerical simulations using AUTODYN and CTH programs were used to design the geometries and predict the impact conditions. A series of experiments were then performed at varying impact velocities to generate a range of deformations while ensuring complete densification. Figure 5 illustrates the anticipated events occurring during dynamic forging, as a rod-shaped powder compact held stationary against an anvil plate, is impacted and squeezed by the projectile. The deformation occurring at high rates results in change in geometry such that the rod- is severely plastically deformed between the anvil plates, eventually forming a hockey-puck shaped powder compact.

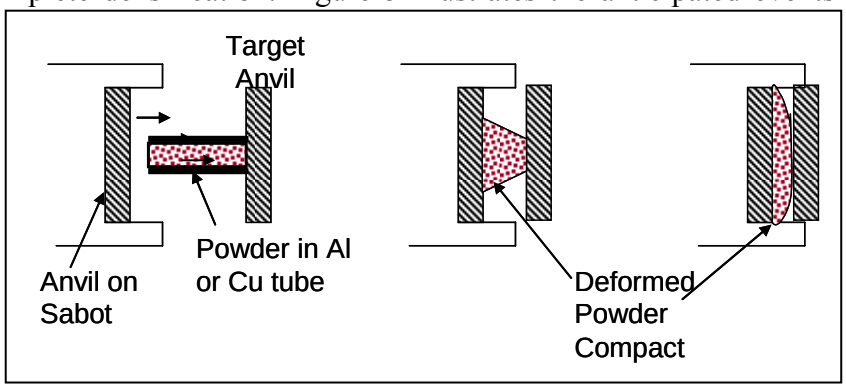


*Fig. 5. Schematic showing series of event occurring during dynamic forging and densification of powder contained in Al or Cu tube.*

Figure 6 below shows an initial design of the experiment. For the first stages of experiment design, typical geometries available in our lab for the sabot and anvil plate were used. Impact was simulated at 800 m/s, close to the impact velocity used for successful shock consolidation.

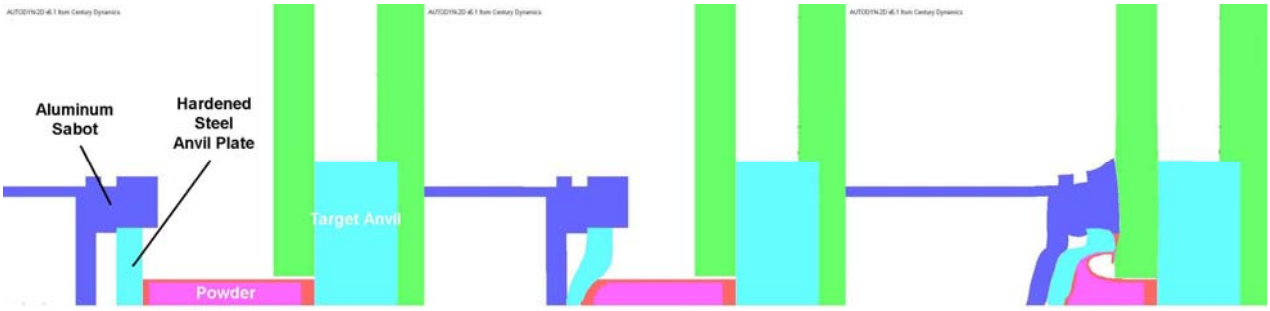


**Fig 6** AUTODYN Simulation of initial experiment geometry at different times.

This simulation showed a high strength steel anvil plate could not be considered as rigid throughout the impact. Further simulations showed better performance for a tungsten anvil plate but revealed that the aluminum sabot lacked the strength to retain the radial flow of the copper and powder. Thus a steel ring was added to contain the sample during forging. This geometry was tested at various velocities to observe the degree of deformation and the final density produced. A simulation showing the final geometry used is shown below in Figure 7.

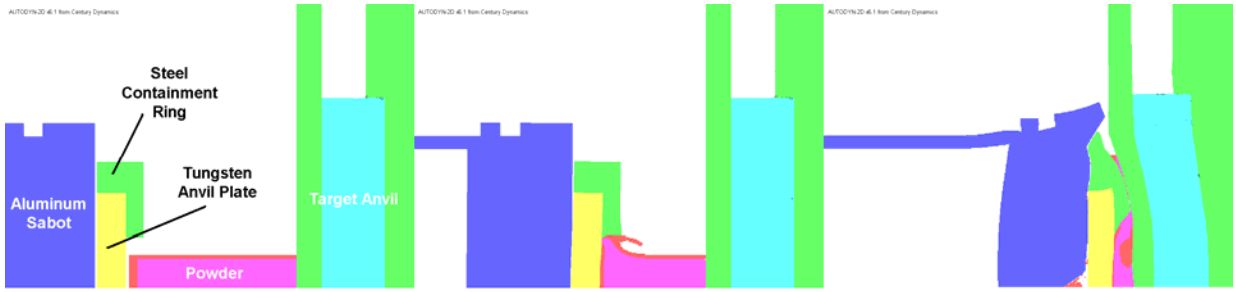


**Fig 7** Simulation results for our first dynamic forging experiment

The impact experiment was performed at 513 m/s on $SmCo_5$, pressed to 43% of TMD in copper tube. Post impact it was found that the sabot and anvil plate had separated from the target plate, thus serving as poor containment. Fragments of the sample were recovered and identified via energy dispersion spectroscopy. An SEM micrograph shown in Figure 8, illustrates that the sample, while fragmented, was fully dense.

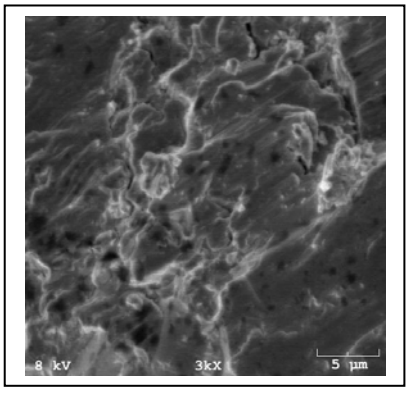


**Fig. 8**. SEM micrograph of recovered sample at 3000X magnification

X-ray analysis was performed on perpendicular faces of the largest fragment, approximately .3 $cm^3$. Figure 9 shows these traces for comparison, zoomed in to the 40 – 47 degree two theta angle range. Overall intensity differences are due mainly to the difference in the size of the faces scanned. Peak profile fitting was used to determine the integrated intensity of each peak. It can be seen that the larger relative intensity of *002* peak in the *j* orientation suggests *002* texture for this sample. While a pole figure analysis is needed to obtain clear evidence of the degree of texture, the preliminary XRD trace peak intensity ratios provide an indication of anisotropy on the severely plastically deformed dynamically forged sample. Magnetic measurements for this sample showed isotropic response.

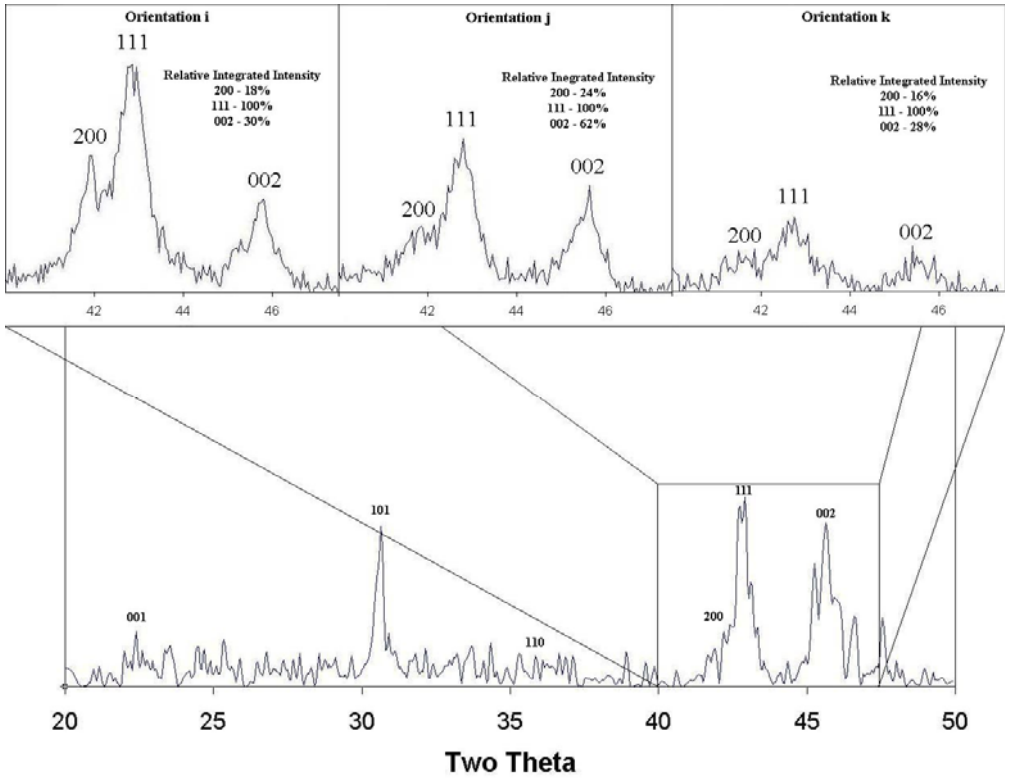


**Fig 9** Typical XRD trace of recovered dynamically forged compact along with a comparison of traces zoomed in the 40 – 47 degree two theta angle range for three different surface orientations. Overall intensity differences are due mainly to the difference in the size of the faces scanned. Peak profile fitting used to determine the integrated intensity of each peak illustrate a larger relative intensity of the 002 peak in the j orientation, suggesting 002 texture for this sample.

The degree of peak broadening suggests a significant reduction in grain size. While a Williamson-Hall plot from these scans did not provide a meaningful estimation of grain size due to the small number of peaks analyzed; TEM imaging of the sample, shown in Figure 10, confirmed a sharp reduction in grain size. It should be noted that these samples were created from a starting powder with a 2-5 micron grain size.

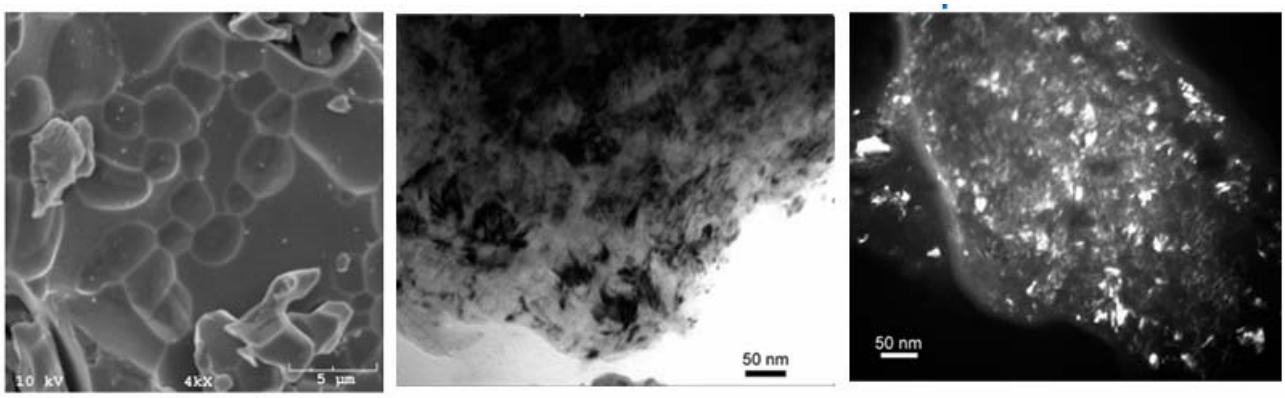


**Fig. 10**. (Left) SEM image of the powder precursor showing 2-5 micon grains. Bright field (Middle) and dark field (Right) images show the post impact microstructure with 20-50 nanometer grains.

The dynamic forging setup was redesigned in an attempt to improve recovery of samples. For this experiment, commercially available $SmCo_5$ powder was pressed into a stainless steel tube to 60% TMD. The tube was mounted to a rigid tungsten anvil inside a radial containment wall. Impact occurred at 304 m/s. Recovery showed that there was poor containment during that experiment and the sample had fractured. The SEM micrograph shown in Figure 11, however, shows good interparticle bonding.

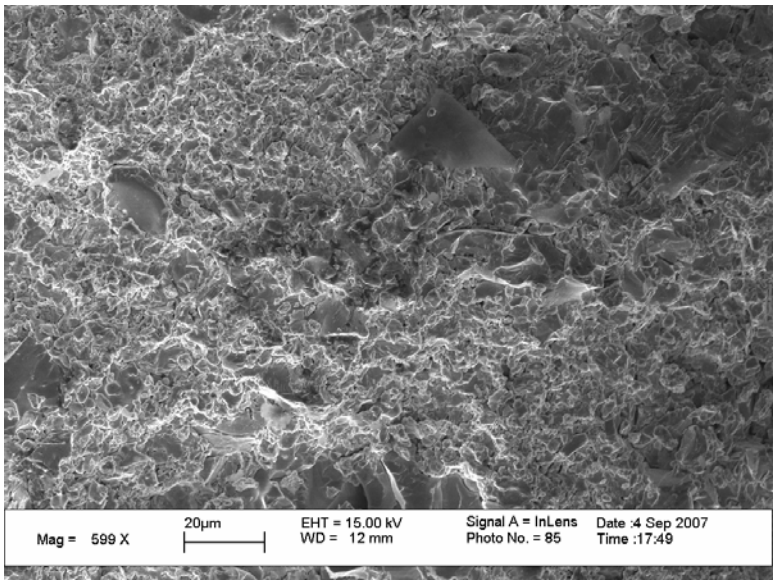


**Fig 11.** Micrograph of recovered compact 07DF2

The compact reached 99% of the TMD. Initial x-ray analysis suggests that the crystallite size is nano-scaled, consistent with the previous experiment. This result is awaiting TEM analysis to be confirmed.

While our numerical simulations can predict deformation behavior, temperature, and pressure, sufficient high strain rate failure models are lacking. We performed several rod-on-anvil impact experiments to help optimize the design of future forging experiments for better recovery. The rod-on-anvil impact tests were performed with SmCo5 powder encased in metal

tubing. Using a 30 caliber gas gun to propel the samples, these experiments had a much faster turn-around time, enabling the testing of several different experimental conditions.

As before, numerical simulations were performed to predict the deformation behavior of the samples. Figure 12 shows a comparison of a simulation with real-time pictures taken of an impact occurring at 205 m/s.

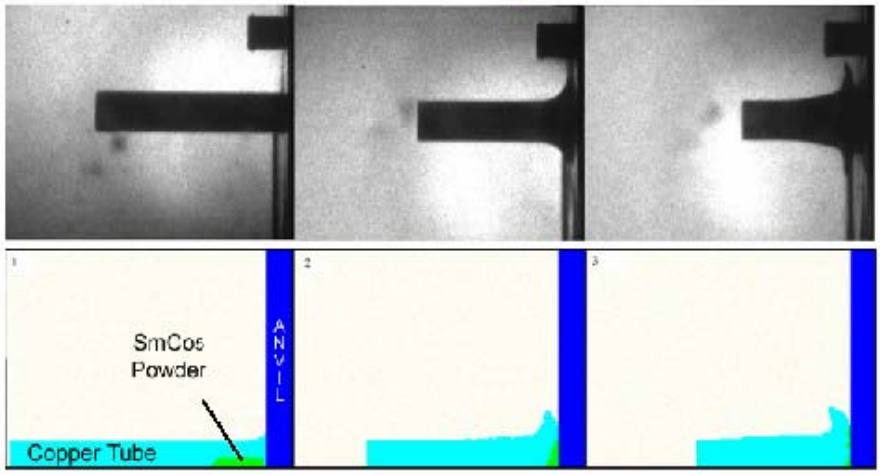


**Fig. 12**. (Top) Real time photographs of impact occurring at 205 m/s.
(Bottom) Simulated results of impact at 205 m/s
The following table summarizes the results of these rod-on-anvil tests.

**Table 2**. Summary of rod-on-anvil tests performed under various impact conditions.

| Impact velocity | Tube | Powder L/D Ratio | Initial Density | Recovery |
|---|---|---|---|---|
| 518 | Steel-A681 | 10 | 48% | Fragmented |
| 492 | SS304 | 10 | 70% | Fragmented |
| 305 | SS304 | 10 | 55% | Fragmented |
| 353 | Copper | 10 | 42% | Intact |
| 410 | SS304 | 2 | 62% | Fragmented |
| 410 | Copper | 2 | 60% | Petaled |
| 317 | Copper | 2 | 57% | Intact |
| 263 | Copper | 2 | 49% | Intact |
| 205 | Copper | 2 | 60% | Intact |
| 93 | Copper | 2 | 60% | No Compaction |

Based on these results, using a copper container with a smaller initial length to diameter ratio is expected to improve recovery of samples. As expected, high impact velocities corresponded to larger amounts of deformation. Figure 13 shows photographs of 3 samples impacted at varying speeds.

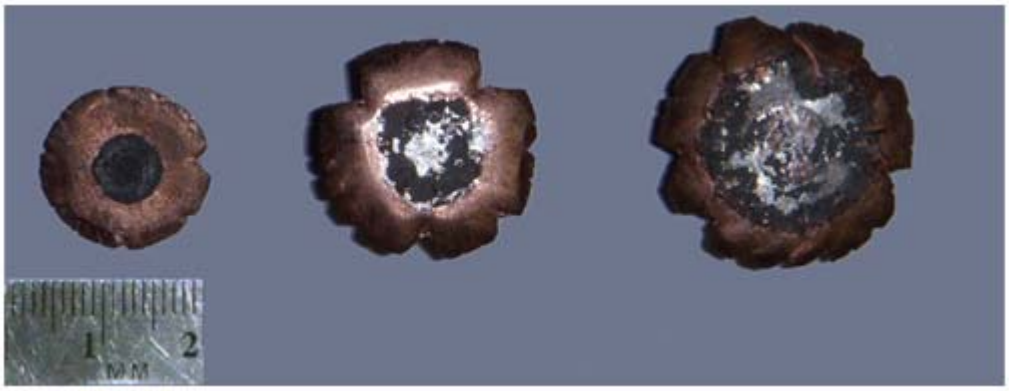


**Fig 13.** Recovered Rod-on-Anvil Specimens impacted at 205, 263, 317 m/s from left to right. Powder is initially 3 mm in diameter.

TEM investigations were peformed on several samples. The TEM images illustrated in Figure 14 showed the presence of both amorphous and nanocrystalline regions, as seen below.

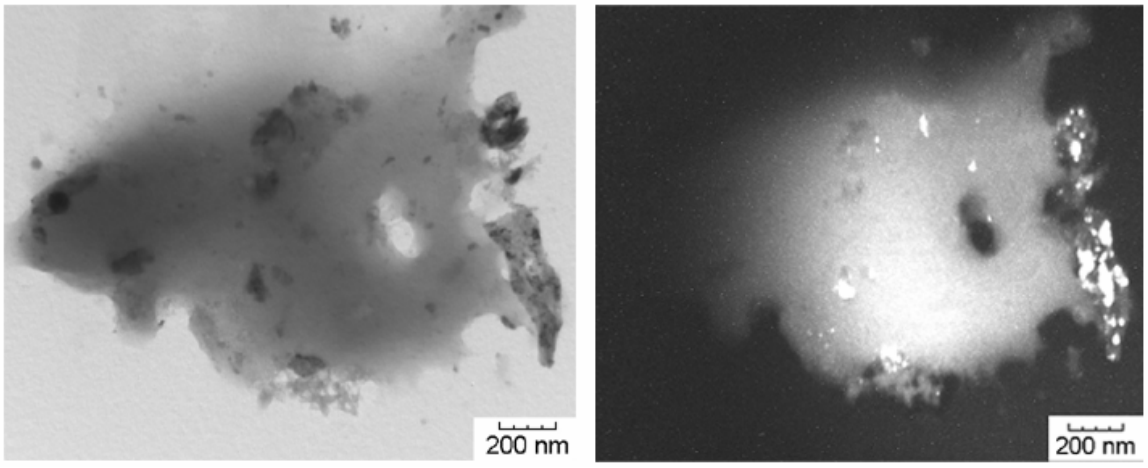


**Fig 14.** Bright field (left) and dark field (right) images of recovered SmCo5 impacted at 263 m/s.

The better recovery of these samples enabled four axis goniometer measurements for pole figure determination despite the significant peak broadening from grain size reduction. Figure 15 below illustrates the effect of increasing deformation during impact on texture development.

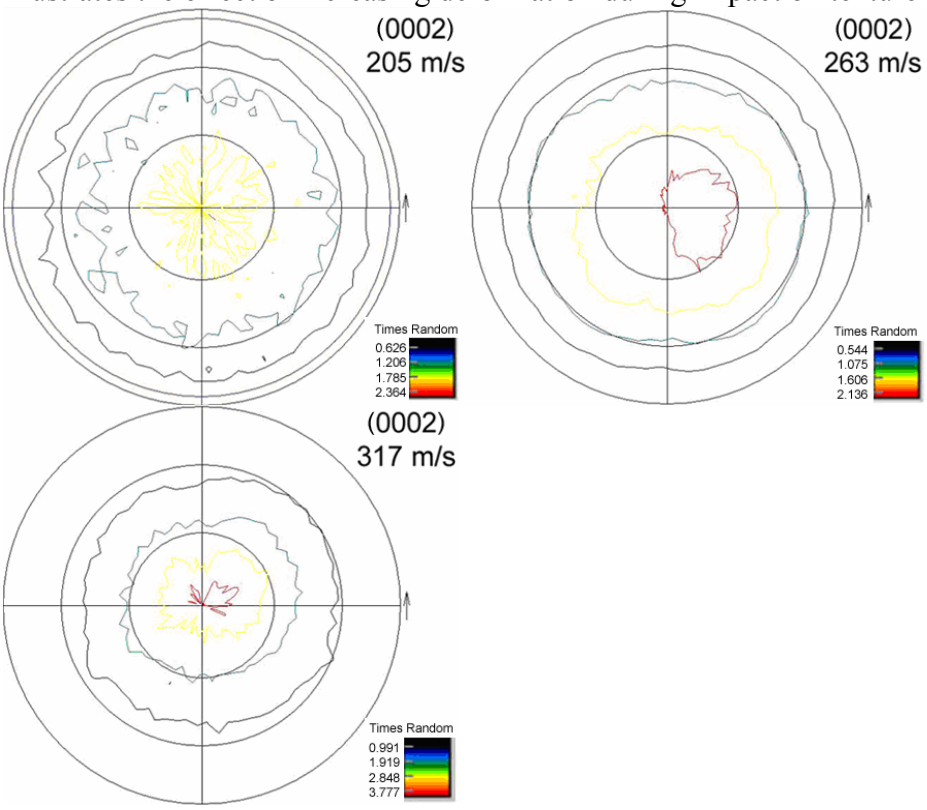


**Fig 15.** (0002) Pole figures of recovered SmCo5 compacts with impact speeds as shown. A sharper fiber texture is seen in the 317 m/s impact than the slower impacts.

## 3.3 Dynamic Extrusion Experiments

Dynamic extrusion experiments concomitant with shock compaction were initially planned to be performed using the sabot and target geometry illustrated schematically in Figure 16, in which a rod-shaped powder compact (pressed in Cu or Al tube) mounted on Al-sabot is accelerated to pass through an angular die, resulting in >100% reduction in cross-sectional area.

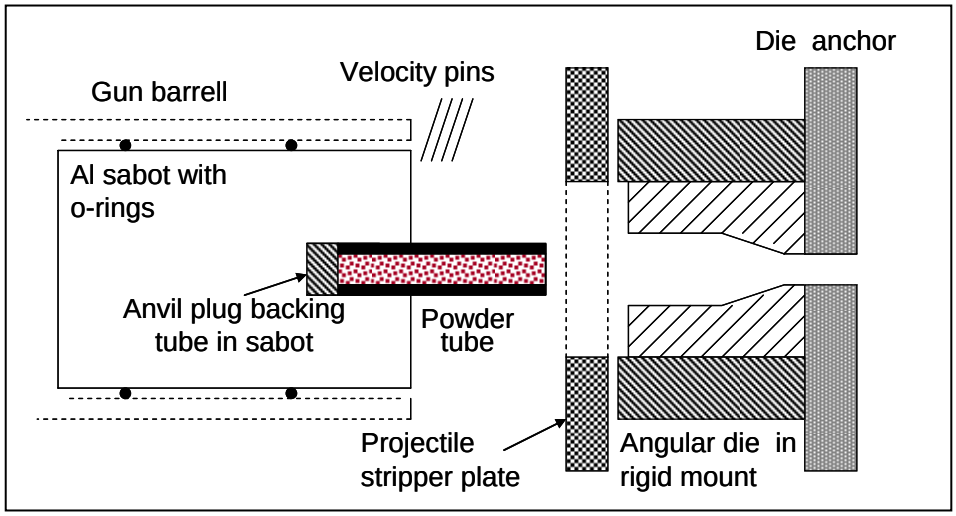


*Fig. 16. Schematic of sabot/target geometry to be employed for dynamic extrusion experiments.*

The experiments were to be performed at varying impact velocities to generate a range of deformation conditions while ensuring complete densification, with the desired impact velocity range determined based on two- and three-dimensional numerical simulations using AUTODYN and CTH programs. Figure 17 illustrates the anticipated pattern of deformation during dynamic extrusion, as the rod-shaped compact is reduced in cross-section through an angular die.

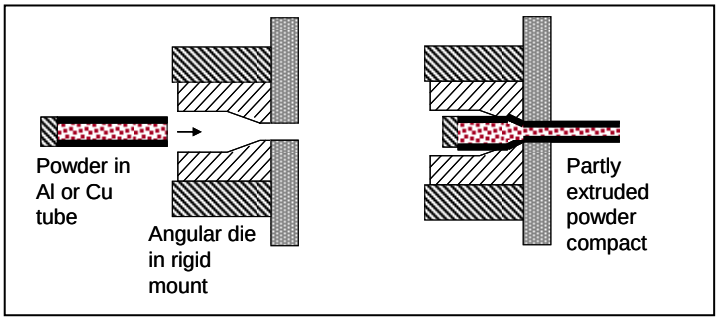


*Fig. 17. Schematic showing series of events during extrusion.*

It was realized that the overall momentum with this design would be too high, making it difficult to enable stripping of the sample from the sabot. As such, a new 30-caliber gas gun was acquired for performing the dynamic extrusion experiments. The design of the dynamic extrusion die was performed using AUTODYN-2D hydrocode, with the following design parameters: material, drawing angle, bore size, bearing length, and relief angle. Based on the results the simulation work, the die shown schematically in Figure 18, was made from tungsten carbide, Class C-14, with a drawing angle of 14 degrees (28 degrees inclusive) and two bore sizes 0.200" and 0.260", which result in a 56% and 25% reduction in the cross-sectional area, respectively. The simulations indicate 100% of the TMD is reached when the specimen undergoes a 50-60% reduction in cross-sectional area. While the bearing length and relief angle were found to be less critical in the densification of the powder, these parameters will be 0.250"

and 20 degrees (40 degrees inclusive), respectively. To mitigate radial expansion of the die, it was interference fit into an AISI 4140 alloy steel casing.

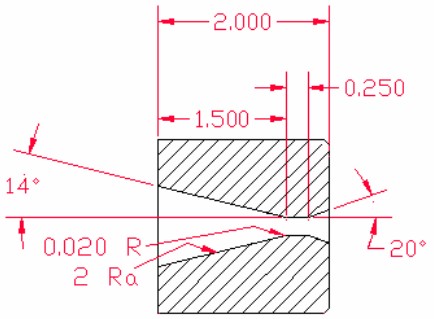


**Fig 18.** Schematic of Dynamic Extrusion Die

The dynamic forging and extrusion methods developed in this work provide an approach for fabrication of fully dense anisotropic nanocomposite bulk magnets with excellent magnetic properties. Development of high performance permanent magnets has been an important fundamental subject for civil applications as well as defense investment strategies for applications, including wave guides for radar, magnetic flywheel bearings, drive transmission chip collectors, positioning motors, electro magnetic interference shielding, hybrid motor pumps and electrically driven platforms which need to perform flawlessly and with reduced noise and vibration. Exchange coupled nanocomposite magnets, with potentially unprecedented magnetic strength, can lead to revolutionary capabilities relevant to Naval service needs, especially for all electric warships and aircraft programs. Magnetic nanocomposites are engineered materials constructed in a way that hard magnetic materials with high coercivity and soft magnetic materials with high saturation magnetization are combined in hybrid magnets to achieve a high magnetic energy product for energy-storage purposes. More than 50 percent power enhancement compared to current magnets can be expected if the aligned nanostructure is well controlled and anisotropic nanocomposites are available. Small rare-earth content also allows for significant reduction in production cost while providing better corrosion resistance and fracture toughness.

[1] Kneller E.F.; Hawig R. The exchange-spring magnet - a new material principle for permanent-magnets, IEEE T Magn. **1991**, 27 (4), 3588-3600.

[2] Z. Q. Jin, K. H. Chen, J. Li, H. Zeng, S.-F. Cheng, J. P. Liu, Z. L. Wang, and N. N. Thadhani: Shock compression response of magnetic nanocomposite powders. Acta Mater. 52 (2004) 2147-2154.

[3] Jin ZQ, Thadhani NN, McGill M, Ding Y, Wang ZL, Chen M, Zeng H, Chakka VM, Liu JP, Explosive shock processing of $Pr_2Fe_{14}B/\alpha$-Fe exchange-coupled nanocomposite bulk magnets. J MATER RESEARCH, Vol. 20, No. 3, 599-609, Mar 2005